J Mater Sci: Mater Electron
DOI 10.1007/s10854-017-7599-6

Improvement on dielectric and microstructural properties of lead free $Bi_{0.5}Na_{0.5}TiO_3$ ceramics through processing conditions

Andrea Prado-Espinosa[1] · Javier Camargo[1] · Leandro Ramajo[1] · Miriam Castro[1]

Received: 27 June 2017 / Accepted: 22 July 2017

Abstract In this work, we report the influence of processing conditions on $Bi_{0.5}Na_{0.5}TiO_3$-based lead–free piezoceramics properties, obtained by conventional solid-state reaction method, employing a mechanochemical activation step and comparing two types of calcination steps. All samples were characterized by X-ray diffraction, Scanning Electron Microscopy and impedance Spectroscopy. It was observed that depending on the calcination route a secondary phase is formed. Moreover, the content of the secondary phase is strongly related to the intermediate grinding in the calcined process, and has a significant effect on the final ferroelectric properties.

1 Introduction

$Bi_{0.5}Na_{0.5}TiO_3$ (BNT) is a ferroelectric material with perovskite structure and rhombohedral phase at room temperature. It presents a high Curie temperature, around 320 °C, and a large remnant polarization (38 μC/cm^2) [1]. Furthermore, by its good ferroelectric properties, BNT could replace lead zirconate–titanate ceramics (Pb(Zr,Ti)O_3–PZT), in many applications such as sensors, actuators, and transducers due to their electromechanical properties [2–4], because of PZT has a high amount of lead oxide (PbO) which is toxic and produces serious environmental problems [5, 6]. Therefore, in order to reproduce the excellent properties of traditional piezoelectric materials, enormous research efforts are focus on the study and development of lead free materials as a possible solution, ceramics exhibiting piezoelectric properties, such as bismuth sodium titanate BNT, $Bi_{0.5}K_{0.5}TiO_3$ and potassium sodium niobate $K_{0.5}Na_{0.5}NbO_3$ have been studied [7, 8].

The main problem of BNT ceramics is the high coercive field and high conductivity that is affected by the existence of secondary phase and by the volatilization of bismuth ions in the sintering process [9, 10]. Consequently, the formation of secondary phases and the elimination of volatile elements (e.g. bismuth) should be avoided by controlling the grinding process, the powder calcination and the sintering process. In order to avoid the formation of secondary phases, Suvorov and colleagues implemented an intermediate milling step in the calcination process [11]. They found that a better homogeneity of the perovskite phase can be achieved with multiple high-temperature firings. However, irrespective of the firing conditions, they could not obtain single-phase ceramics.

Taking into account previous results and regarding the formation of secondary phases, in this work two calcination steps were analyzed. Lead free powders (BNT) were synthesized through the solid-state reaction method, employing a mechanochemical activation step and two different types of calcination processes. Finally, samples were sintered and final properties were measured. It was observed that the secondary phase formation in sintered ceramics depended on the previous calcination route.

2 Experimental procedure

BNT was prepared by conventional solid-state reaction method, employing a mechanochemical activation step, using Na_2CO_3 (Cicarelli 99.99%; Argentina), Bi_2O_3

✉ Andrea Prado-Espinosa
apespinosa@fi.mdp.edu.ar

[1] Institute of Research in Materials Science and Technology (INTEMA), Juan B. Justo 4302, Mar del Plata B7608FDQ, Argentina

Published online: 27 July 2017

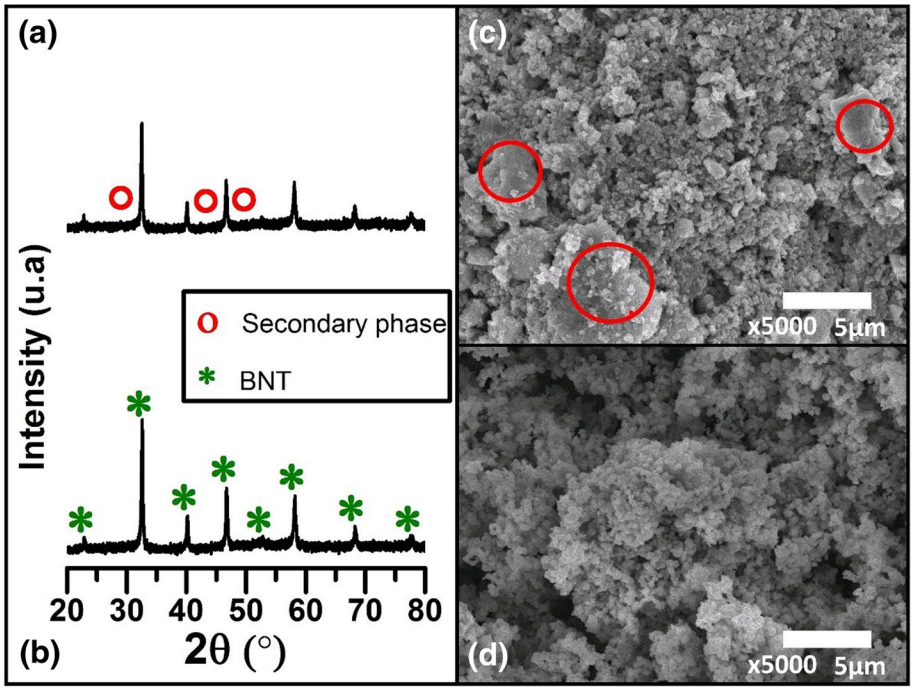

Fig. 1 XRD patterns and SEM images of calcined powders at 750 °C for 2 h; **a, c** corresponding to Method 1, **b, d** to Method 2. Peaks associated with the presence of secondary phase (symbol "O") can be observed. (Color figure online)

(Aldrich 99.8%; USA), and TiO_2 (Aldrich 99.9%; USA). Powders were mixed and milled using zirconia balls in an alcoholic medium for 6 h in a planetary mill (Fritsch, Pulverisette 7, 1450 rpm). Following Suvorov and colleagues' method [11], powders were prepared by two alternative routes, in the first route powders has been calcined in two steps, each one of 1 h at 750 °C, separated by a grinding step of 2 h in alcoholic medium (Method 1). In the second route, powders were directly calcined at 750 °C by 2 h (Method 2). Powders were pressed into disks and sintered at 1150 °C for 2 h.

Crystalline phases were characterized by X-ray diffraction (XRD) DRX, PANalytical, X'pert Pro, Cu Kα. Microstructures were evaluated on polished and thermally etched samples by Scanning Electron Microscopy (SEM) using a JEOL JSM-6460LV microscope equipped with energy dispersive spectroscopy, EDS. Density values were determined by the Archimedes' method.

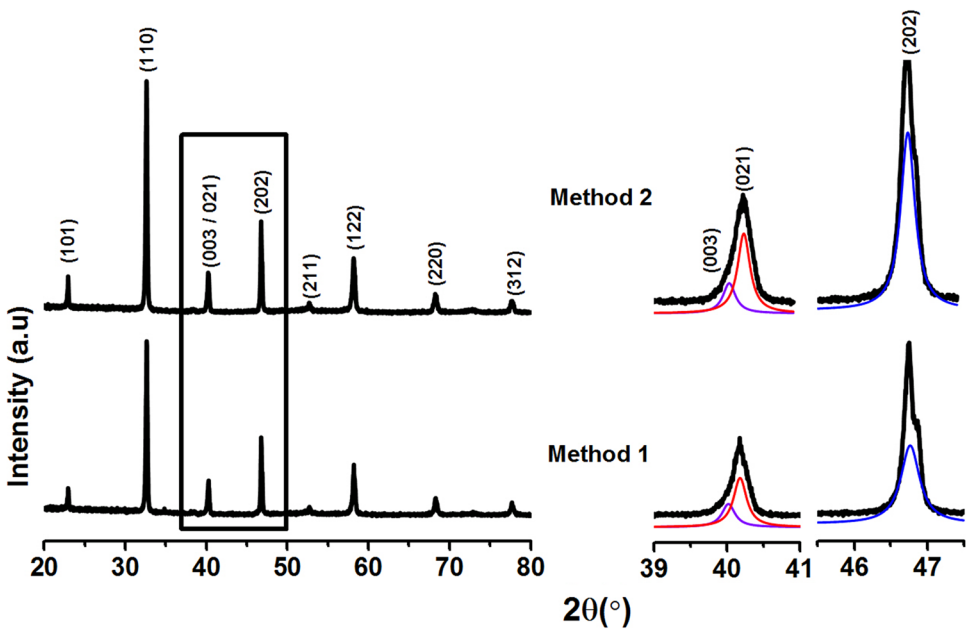

Fig. 2 XRD patterns of sintered samples at 1150 °C for 2 h of BNT employing both calcination methods. The inserts of each figure show a detail of the XRD pattern in the 2θ range 39°–41° and 45°–48° of the BNT

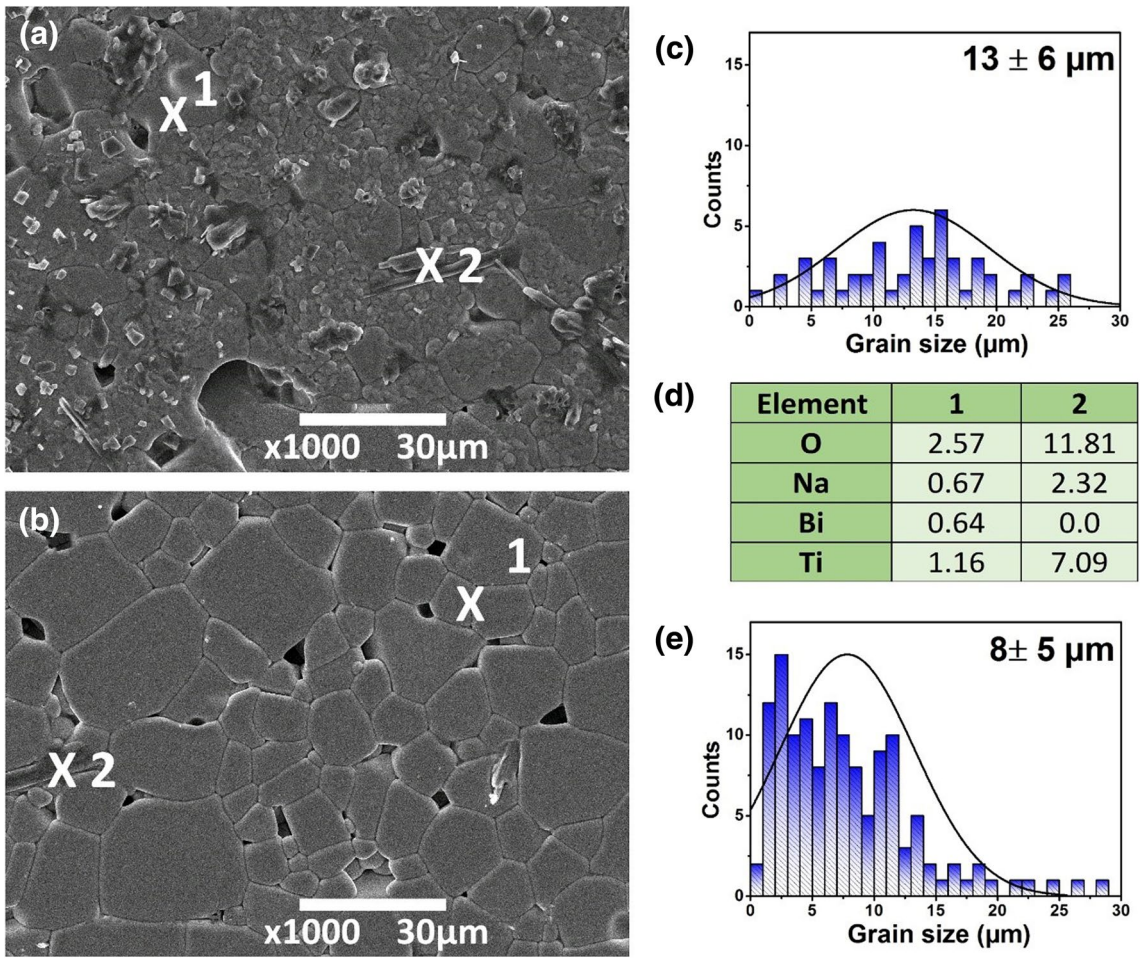

Element	1	2
O	2.57	11.81
Na	0.67	2.32
Bi	0.64	0.0
Ti	1.16	7.09

Fig. 3 SEM micrographs of BNT sintered at 1150 °C for 2 h and processed by **a** Method 1 and **b** Method 2. The inserts of **c, e** show the average grain size (AGS) of BNT ceramics, and the insert **d** lists the compositions of the points shown on micrograph derived from EDS spectra. The table represents the atomic percentages of elements

Previous to the electrical measurements, samples were painted using a fired silver paste for the electric contacts. The temperature dependence of the dielectric properties was determined using an impedance analyzer (Hewlett–Packard, HP4284A) over a frequency range of 20 Hz–1 MHz. Samples were polled in a silicone oil bath at 100 °C by applying a DC field of 30.0 kV/cm for 10 min. The polarization–electric field (P–E) hysteresis loops were measured in a silicon oil bath using a modified Sawyer–Tower circuit, the piezoelectric constant d_{33} was measured using a piezo d_{33} meter (YE2730A d_{33} METER, APC International, Ltd., USA). The electromechanical coupling factors (Kp) and (Kt) were calculated from the impedance curves of the polarized ceramics, according to equations [12].

$$K_p = \sqrt{2.51 \times \left(\frac{(f_a - f_r)}{f_a}\right)} \quad (1)$$

$$K_t = \sqrt{\frac{\pi}{2}\frac{f_r}{f_a}\tan\frac{\pi}{2}\left\{\frac{(f_a - f_r)}{f_a}\right\}} \quad (2)$$

3 Results and discussion

Figure 1a, b shows the XRD patterns of the calcined powder at 750 °C for 2 h with and without intermediate grinding. It can be seen, that all the diffraction patterns correspond to a perovskite-phase with rhombohedral structure and lattice parameters a, b and c 5.476, 5.476, 6.778 (Å), respectively (JCPDS No. 36-340). As it was previously reported [13], slight traces of a minor secondary phase, (symbol **O**) assigned to $Na_2Ti_6O_{13}$ (NTO) (JCPDS No. 14-0277) can be observed. Moreover, this secondary phase is more pronounced in powders obtained from a calcined process with intermediate grinding (Method 1). In addition, Fig. 1c, d show the micrographs of calcined powders

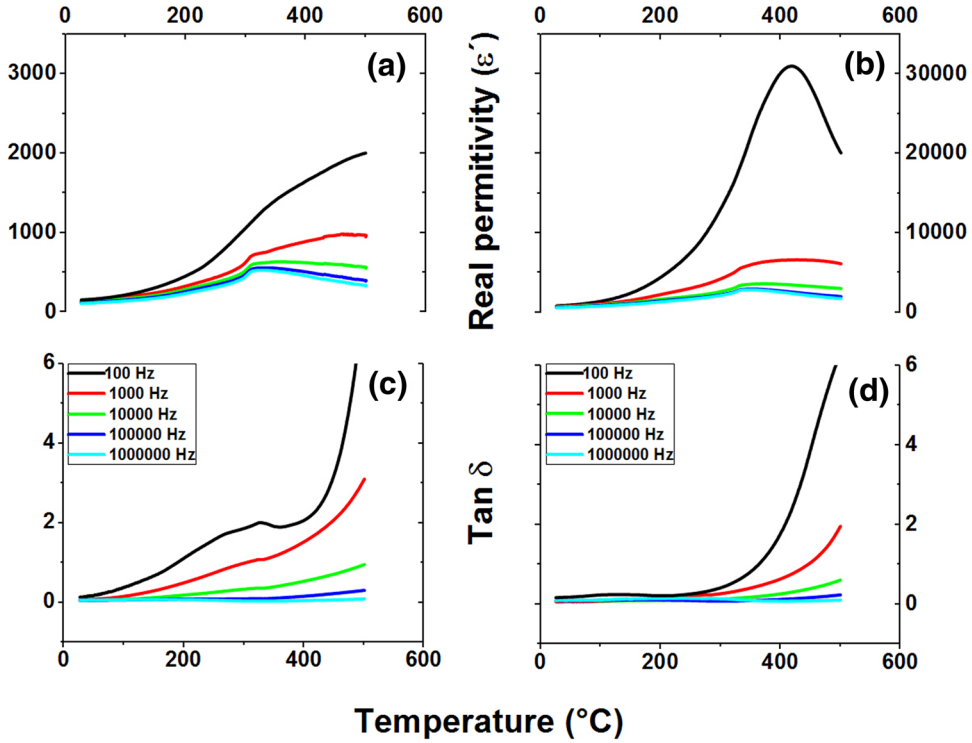

Fig. 4 Real permittivity—**a** Method 1, **b** Method 2 and dielectric loss—**c** Method 1, **d** Method 2 versus temperature curves of BNT-1150 °C samples obtained at different frequencies

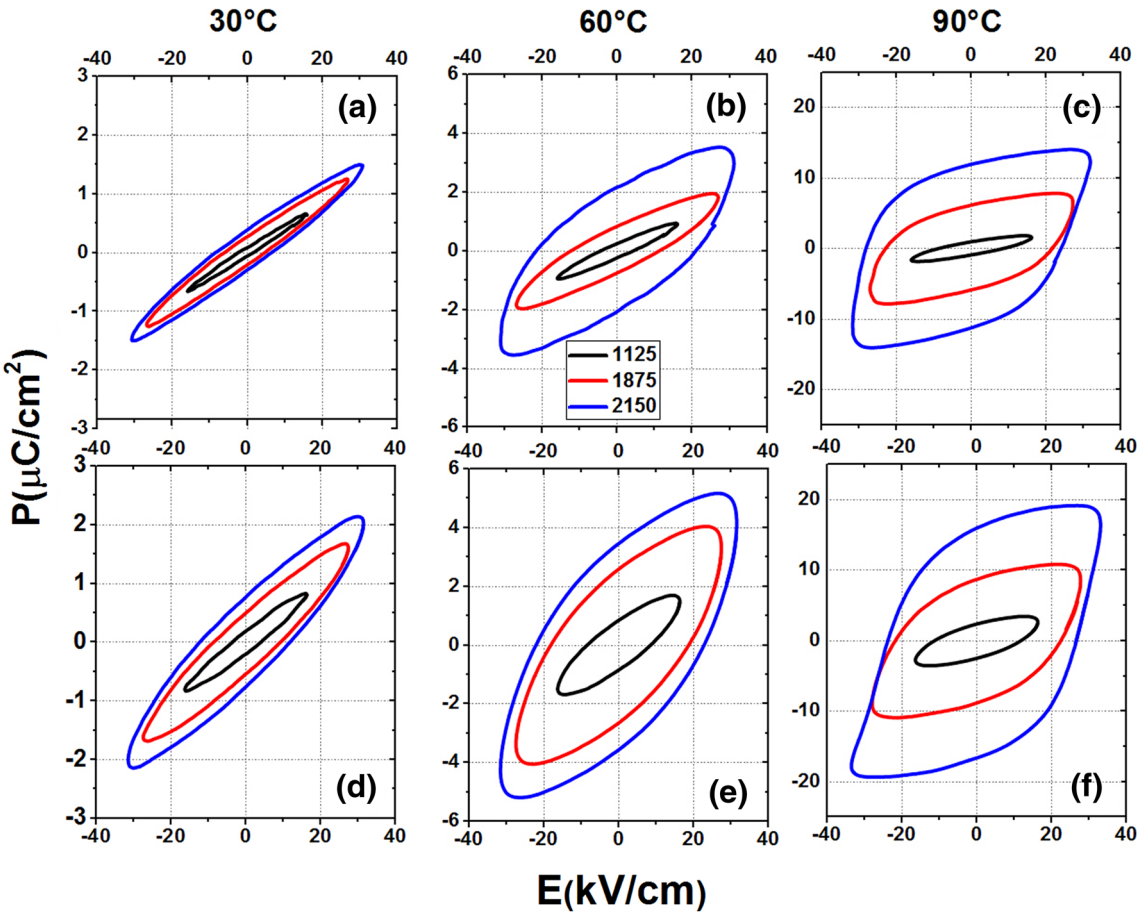

Fig. 5 P–E hysteresis loops of BNT ceramics as a function of temperature, **a–c** Method 1, and **d–f** Method 2

Table 1 The relative density (ρ), piezoelectric coefficient (d_{33}), dielectric constant (ε') and loss tangent (tanδ) and electromechanical coupling coefficient (kp and kt), of the BNT ceramic samples measured at 30 °C and 10 kHz

Sample	ρ (g/cm^3)	d_{33} (pC/N)	ε'	tan (δ)	Kp	Kt
Method 1	5.66	35	124.93	0.05487	–	–
Method 2	5.79	80	640.68	0.05168	0.21	0.15

from both methods. In Fig. 1c the presence of blocks (red circles) associated with the presence of a secondary phase can be observed, as it was previously detected from XRD patterns, while Fig. 1d displays a homogeneous microstructure without the presence of secondary phases, indicating that calcination step influences the formation of secondary phases.

The XRD patterns of calcined powders at 750 °C and sintered at 1150 °C using both calcination methods are shown in Fig. 2. It can be observed, in both cases, that a main phase corresponding to the BNT-phase, free of secondary phases, is detected, while peaks located between $39° < 2\theta < 41°$ and $45° < 2\theta < 48°$ corresponding to (003), (021) and (202) are fitted to the sum of two Lorentzian peaks indicating the stabilization of the pure rhombohedral structure for both routes.

Figure 3 shows the microstructure of sintered samples at 1150 °C, for both calcination methods. A regular grain growth and the formation of a secondary phase, which appears in surface in form of rods, after the sintering process are registered in samples obtained from Method 1 (Fig. 3a). Although the NTO phase was previously registered in powders where intermediate grinding steps were included in the calcination process [13] (Method 1) morphology (dimensions and shape) was modified during the sintering process. Furthermore, this secondary phase was also observed in sintered samples obtained through Method 2 (Fig. 3b). Through EDS analysis, the composition of the secondary phase was determined. This phase resulted rich in sodium and poor in bismuth, and the content decreased considerably from Method 1 to Method 2 (Fig. 3d).

The AGS of sintered samples is shown in Fig. 3c, e. It can be observed that employing the first method, the grain size distribution is wide (AGS 13 ± 6 μm), whereas samples prepared using the Method 2 displayed a low content of secondary phases and an AGS of 8 ± 5 μm. It can be suggested that the intermediate grinding step employed in Method 1 increased the powder reactivity, favoring the alkaline evaporation and the grain growth.

Relative permittivity and the dielectric loss as a function of temperature at various frequencies of samples sintered at 1150 °C is shown in Fig. 4. A representative peak around of 400 °C is associated with the phase transition anti-ferroelectric to paraelectric (T_m), while the transition temperature from ferroelectric to anti-ferroelectric (T_d) does not show a representative peak. On the other hand, samples without intermediate grinding present higher values of permittivity than the other set of samples (Fig. 4b), these values exceed in one magnitude order to the samples with intermediate grinding (Fig. 4a), we believe that this behavior is related to the amount and distribution of NTO phase into the samples [13]. Moreover, dielectric losses increase in samples with intermediate grinding in the calcined process (Fig. 4c). In previous works, it was reported that the presence of the secondary phase (NTO) modifies the electric properties of BNT ceramics [9].

Dielectric hysteresis at different temperatures of BNT samples with and without grinding intermediate are shown in Fig. 5. Samples produces employing the first method, Fig. 5a, c, present a remnant polarization of 0.387 μC/cm^2 at 30 °C which increases until 11.97 μC/cm^2 at 90 °C, while the coercive field values oscillated between 6.41 and 23.84 kV/cm^2 when temperature increases from 30 to 90 °C. Samples obtained from the second method, registered higher values (see Fig. 5d, f). Certainly, in these samples remnant polarization and coercive field values change from 0.77 μC/cm^2 and 11.76 kV/cm^2 at 30 °C to 15.99 μC/cm^2 and 26.59 kV/cm^2 at 90 °C. For both methods, a transformation from a soft to a hard-ferroelectric material with increment of temperature is registered.

Finally, Table 1 shows density (ρ), piezoelectric coefficient (d_{33}), real permittivity (ε'), loss tangent (tan(δ)) and electromechanical coupling coefficient values of these samples. In general, the measured values are similar to the ones registered by other authors [14]. Specimens prepared without an intermediate grinding, present the highest properties. Electromechanical coupling was not measured in samples obtained by the first method, due to their low density and piezoelectric coefficient values.

4 Conclusions

Microstructure and ferroelectric properties of BNT ceramics were modified using two calcination routes. In the first method powders were calcined in two steps, separated by a grinding step. In the second route, powders were directly calcined. XRD and SEM results showed that the grinding intermediate step favors the formation of a NTO secondary phase. Sintered samples obtained from the first method

displayed a secondary phase which was overall distributed. Moreover, the implementation of the second method (calcination in one step) avoids the formation of the secondary phase and improves dielectric and ferroelectric properties of BNT ceramics.

Acknowledgements The authors thank the following institutions for providing financial support: National Research Council (CONICET, Argentina) Project PIP 2012-0432, University of Mar del Plata (Argentina) Project (15G/388) and National Agency for Scientific and Technological Promotion (ANPCyT) PICT 2014-1314.

References

1. B.-J. Chu, D.-R. Chen, G.-R. Li, Q.-R. Yin, Electrical properties of $Na_{1/2}Bi_{1/2}TiO_3$–$BaTiO_3$ ceramics. J. Eur. Ceram. Soc. **22**, 2115–2121 (2002). doi:10.1016/S0955-2219(02)00027-4
2. E. Ringgaard, T. Wurlitzer, Lead-free piezoceramics based on alkali niobates. J. Eur. Ceram. Soc. **25**, 2701–2706 (2005). doi:10.1016/j.jeurceramsoc.2005.03.126
3. H. Birol, D. Damjanovic, N. Setter, Preparation and characterization of $(K_{0.5}Na_{0.5})NbO_3$ ceramics. J. Eur. Ceram. Soc. **26**, 861–866 (2006). doi:10.1016/j.jeurceramsoc.2004.11.022
4. D. Lin, K.W. Kwok, H.L.W. Chan, Structure and electrical properties of $Bi_{0.5}Na_{0.5}TiO_3$–$BaTiO_3$–$Bi_{0.5}Li_{0.5}TiO_3$ lead-free piezoelectric ceramics. Solid State Ionics **178**, 1930–1937 (2008). doi:10.1016/j.ssi.2007.12.096
5. V. Schmitt, F. Raether, Effect of cobalt doping on the sintering mechanisms of the lead-free piezoceramic (Bi0.5Na0.5) TiO3. J. Eur. Ceram. Soc. **34**, 15–21 (2014). doi:10.1016/j.jeurceramsoc.2013.07.021
6. Directive 2002 95/EC of the European Parliament and of the Council of 27 January 2003 on the restriction of the use of certain hazardous substances in electrical and electronic equipment. Off. J. Eur. Union 2003. L37/19–L37/37.3
7. H. Yu, Z.-G. Ye, Dielectric, ferroelectric, and piezoelectric properties of the lead-free $(1–x)(Na_{0.5}Bi_{0.5})TiO_3$-$xBiAlO_3$ solid solution. Appl. Phys. Lett. **93**, 112902 (2008). doi:10.1063/1.2967335
8. X. Ma, L. Xue, L. Wan, S. Yin, Q. Zhou, Y. Yan, Synthesis, sintering, and characterization of BNT perovskite powders prepared by the solution combustion method. Ceram. Int. **39**, 8147–8152 (2013). doi:10.1016/j.ceramint.2013.03.088
9. L. Ramajo, M. Castro, A. del Campo, J.F. Fernandez, F. Rubio-Marcos, Influence of B-site compositional homogeneity on properties of $(K_{0.44}Na_{0.52}Li_{0.04})(Nb_{0.86}Ta_{0.10}Sb_{0.04})O_3$-based piezoelectric ceramics. J. Eur. Ceram. Soc. **34**, 2249–2257 (2014). doi:10.1016/j.jeurceramsoc.2014.02.002
10. C.C. Jin, F.F. Wang, L.L. Wei, J. Tang, Y. Li, Q.R. Yao et al., Influence of B-site complex-ion substitution on the structure and electrical properties in $Bi_{0.5}Na_{0.5}TiO_3$-based lead-free solid solutions. J. Alloys Compd. **585**, 185–191 (2014). doi:10.1016/j.jallcom.2013.09.152
11. J. König, M. Spreitzer, D. Suvorov, Influence of the synthesis conditions on the dielectric properties in the $Bi_{0.5}Na_{0.5}TiO_3$–$KTaO_3$ system. J. Eur. Ceram. Soc. **31**, 1987–1995 (2011). doi:10.1016/j.jeurceramsoc.2011.04.007
12. J.-F. Trelcat, C. Courtois, M. Rguiti, A. Leriche, P.-H. Duvigneaud, T. Segato, Morphotropic phase boundary in the BNT–BT–BKT system. Ceram. Int. **38**, 2823–2827 (2012). doi:10.1016/j.ceramint.2011.11.053
13. A. Prado-Espinosa, M. Castro, L. Ramajo, Influence of secondary phases on ferroelectric properties of $Bi_{0.5}Na_{0.5}TiO_3$ ceramics. Ceram. Int. **43**, 5505–5508 (2017). doi:10.1016/j.ceramint.2017.01.071
14. B.K. Barick, R.N.P. Choudhary, D.K. Pradhan, Dielectric and impedance spectroscopy of zirconium modified $(Na_{0.5}Bi_{0.5})TiO_3$ ceramics. Ceram. Int. **39**, 5695–5704 (2013). doi:10.1016/j.ceramint.2012.12.087